Applied Chemical Engineering (2025) Volume 8 Issue 3 ISSN: 2578-2010 (O)
doi: 10.59429/ace.v8i3.5729

ORIGINAL RESEARCH ARTICLE

Efficient adsorption of congo red dye from aqueous solution using MWCNT/Chitosan-g-Poly (acrylic acid–crotonic acid) composite

Khudhair M. Mahdi[1], Safaa Abdulkadhim Almansarawi[2], Layth S. Jasim[3] , Maryam Batool[4]

[1, 2] *Department of Chemistry, University of Sumer, College of Education, Thi-Qar, 64011, Iraq*

[3] *Department of Chemistry, College of Education, University of Al-Qadisiyah, Diwaniyah, 58002, Iraq*

[4] *Department of Chemistry, University of Sahiwal, Sahiwal, 57000, Pakistan*

***Corresponding author:** Khudhair M. Mahdi; khudhairmohammed937@gmail.com

ABSTRACT

This research studies the synthesis and evaluation of a new composite material, MWCNT/Chitosan-g-Poly (acrylic acid–crotonic acid), designed for the efficient removal of congo red (CR) dye from water. The composite was created through a graft polymerization technique and characterized by FTIR, XRD, and FE-SEM. These analyses confirmed the successful integration of MWCNTs and presence of numerous functional groups for adsorption. To understand the composite's performance, a series of batch experiments were performed to investigate the impact of contact time, pH, adsorbent dose, and initial dye concentration. Study was best described by pseudo-second model and Langmuir model (with maximum adsorption capacity of 14.13 mg g^{-1}) was the best fit for the equilibrium data and process was thermally spontaneous and exothermic. Overall, the synthesized material showed good adsorption potential for dye removal from water.

Keywords: Congo red (CR) dye; composite; adsorption; water

ARTICLE INFO

Received: 11 August 2025
Accepted: 9 September 2025
Available online: 15 September 2025

1. Introduction

Water pollution has become one of the most critical environmental issues nowadays. Synthetic dyes from industries such are a major source of water pollution, posing a significant threat to aquatic ecosystems and human health [1]. These dyes are complex organic compounds that are often resistant to biodegradation, light, and temperature [2,3]. Even in small concentrations, they can reduce light penetration and disrupt photosynthesis in water system. Furthermore, many dyes and their breakdown products are known to be toxic, mutagenic, and carcinogenic, presenting direct risks to human health through contaminated drinking water [4]. To address these hazards, the effective treatment of dye-laden wastewater is essential. Removing these pollutants before they are released into the environment is vital for complying with environmental laws and protecting water resources for future generations. While various physical, chemical, and biological methods as flocculation, membrane filtration, and ozonation have been developed, many have limitations. These include high operational costs, incomplete color removal, the generation of large amounts of sludge, and reduced efficiency with highly concentrated dye solutions. Among these methods, adsorption has gained considerable attention as a highly effective and versatile approach for

removing dyes from water [5]. The choice of adsorbent is crucial, and a wide variety of materials [7-9].

Carbon nanotubes (CNTs), especially multi-walled carbon nanotubes (MWCNTs), are of great interest due to their exceptional surface area and high adsorption potential. However, pristine MWCNTs tend to clump together due to strong van der Waals forces, which limit their effectiveness. To overcome this, surface functionalization and hybridization with polymers or biopolymers are used to improve adsorption. In this study, a novel composite based on MWCNTs and chitosan, grafted with poly(acrylic acid–crotonic acid) [MWCNT/Chitosan-g-P(AA–CA)], was synthesized for the adsorption of CR dye [10,11]. Grafting with poly (acrylic acid–crotonic acid) improves chitosan's stability and adds more functional groups, enhancing its affinity for anionic dyes [12]. The primary aim of this research is to evaluate the adsorption performance of this novel composite. Unlike earlier chitosan/CNT or chitosan-g-AA materials, our design incorporates additional carboxyl groups from crotonic acid grafting, which significantly strengthens the electrostatic attraction to anionic dyes. Simultaneously, the MWCNTs contribute powerful π–π stacking interactions. The synergy between these two effects leads to higher adsorption efficiency and better stability in acidic solutions.

2. Materials and methods

2.1. Chemicals

The following chemicals were purchased and used as received: multi-walled carbon nanotubes-carboxyl (95%), crotonic acid, chitosan (99%) and acrylic acid (99%), potassium persulfate (99%), n,n'-methylene-bis-acrylamide (99%), nitrogen gas, sodium hydroxide (99% purity), hydrochloric acid (36%), and CR dye (99%).

2.2. Instrumentation

The Shimadzu UV-Visible Spectrometer and a Shimadzu FTIR employed for spectroscopic analysis. Morphological characterization was performed using a TESCAN Field Emission-Scanning Electron Microscope (FESEM, Model MIRA3) at 15 kV with gold sputter-coating. Other key equipment included an X-ray diffraction Spectroscopy (Model XRD-6000, Shimadzu), a Trup International Centrifuge (Model 80-1), a Jlabtech Shaker Incubator (Model LSI-3016A), and a Denova Electronic Balance (Model L420 B). An Intertek pH meter (Model pH-3110), a Jlabtech Oven (Model L-OD-380N), and a Hotplate (Model L-81, Labtech) were also employed. For water purification and temperature control, a Water Still, a Labtech Ultrasonic bath (Model LUC - 410), and a Labtech Water Bath (Model K-WBBL) were utilized.

2.3. Preparation of MWCNT/CS-g-P(AA-CA) nanohydrogel composite

The MWCNT/CS-g-P(AA-CA) nanohydrogel composite was prepared through a sequence of solution-based steps. Initially, a 1% acrylic acid (AAc) solution was obtained by diluting 0.5 mL of concentrated AAc to 50 mL with distilled water, from which 20 mL was used in the reaction. Separately, 0.5 g of chitosan (Ch) was dissolved in 20 mL of acetic acid under magnetic stirring for 15 minutes, while 0.1 g of multi-walled carbon nanotubes (MWCNTs) was dispersed in 100 mL of distilled water. Both solutions were then combined, followed by the addition of 5 mL of crotonic acid (CA), previously prepared by dissolving 1 g of CA in 5 mL of distilled water. The mixture was stirred for another 15 minutes before adding 5 mL of AAc and continuing the stirring for an additional 15 minutes. A crosslinking agent solution was prepared by dissolving 0.05 g of N, N′-methylenebisacrylamide (MBA) in 2 mL of distilled water, and an initiator solution was prepared by dissolving 0.05 g of potassium persulfate (KPS) in 2 mL of water. Both solutions were added dropwise to the reaction mixture under stirring. The entire solution was then subjected to ultrasonication for 1 hour, followed by nitrogen gas purging for 1 minute to eliminate dissolved oxygen. The resulting mixture was transferred into test tubes and placed in a water bath at 70 °C for 3 hours to complete the polymerization process. Finally, the

synthesized nanohydrogel was collected, cut into pieces, washed thoroughly with distilled water, and dried in an electric oven at 70 °C [13].

2.4. Batch adsorption study, kinetic, isotherm and thermodynamic models

Fo understanding the effect of dye adsorption on prepared composite, different experiments were performed in batch mode. The dye's adsorption capacity and removal efficiency was calculated using Eq. 1 and 2 correspondingly:

$$Qe \text{ or } \frac{x}{m} = \frac{V(Co-Ce)}{m} \quad (1)$$

$$E\% = \frac{(Co-Ce)}{Co} \times 100 \quad (2)$$

where: C_o ($mg.L^{-1}$) and C_e ($mg.L^{-1}$) refers to initial and equilibrium dye concentrations, respectively, and x is amount of dye adsorbed, whereas m (g) is mass of the adsorbent material and Qe ($mg.g^{-1}$) is amount of dye adsorbed at equilibrium [14,15]. The kinetics of adsorption process were evaluated using two primary models. The pseudo-first model (Eq. 3) states that adsorption rate is directly proportional to the concentration of available, unoccupied active sites. In contrast, the pseudo-second model (Eq. 4) proposes that rate-limiting step involves chemisorption. Further, for understanding equilibrium behavior, several isotherm models were applied. The Langmuir model (Eq. 5) is founded on the premise of monolayer adsorption on a uniform surface where all sites are identical and there are no interactions between adsorbed molecules. Conversely, the Freundlich model (Eq. 6) is an empirical equation used to describe adsorption on heterogeneous surfaces that have sites with different affinities. The Temkin model (Eq. 7), meanwhile, accounts for the interactions between the adsorbent and adsorbate, and assumes that heat of adsorption decreases linearly with increasing surface coverage. Furthermore, the thermal behaviour of the adsorption process was studied by applying thermodynamic model and Van't Hoff plot (ln K_d versus reciprocal absolute temperature). From this plot, the values of enthalpy (ΔH), entropy (ΔS), and Gibbs free energy (ΔG) changes were determined using Equations (8-10) [14,16,17]:

$$\ln (q_e - q_t) = \ln(q_e) - k_1 \cdot t \quad (3)$$

$$\frac{1}{q} = \frac{1}{k2.qe2} + \frac{t}{qe} \quad (4)$$

$$\frac{1}{q_e} = \frac{1}{q_{max}} + \frac{1}{q_o b C_e} \quad (5)$$

$$\log q_e = \log K_f + \frac{1}{n} \log C_e \quad (6)$$

$$q_{eq} = B \ln A_T + B \ln C_{eq} \quad (7)$$

$$\Delta G = \Delta H - T.\Delta S \quad (8)$$

$$\Delta G = -RT \ln K_{eq} \quad (9)$$

$$\ln Keq = -\frac{\Delta H}{RT} + \frac{\Delta S}{R} \quad (10)$$

By applying the kinetic, isothermal and thermal models, the adsorption behaviour of CR dye on studied material can be better analyzed.

3. Results and discussion

3.1. Calibration curve

A robust linear correlation was observed between the concentration of CR dye and its corresponding absorbance values, as depicted by the calibration curve (**Figure 1)**. The high coefficient of determination, with

an R^2 value of 0.9996, underscores reliability of using UV-Vis spectroscopy for accurately quantifying unknown concentrations of Congo Red, confirming the method's suitability for precise measurements.

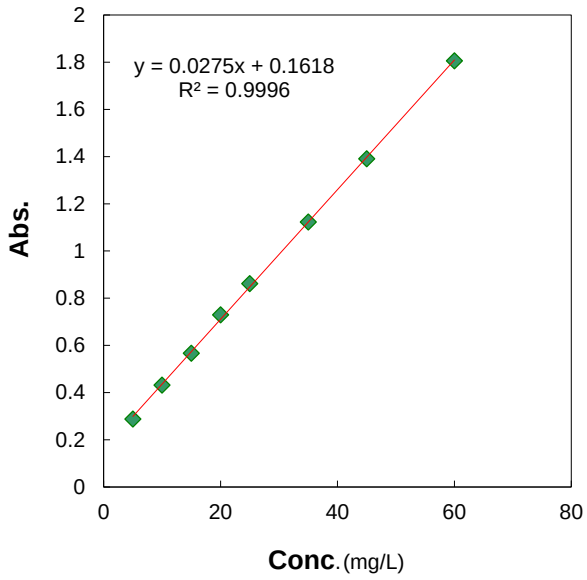

Figure 1. Calibration of CR dye

3.2. Characterization findings

The FTIR (**Figure 2)** of MWCNT/Chitosan-g-P(AA–CA) composite prior to adsorption showed key peaks. A broad band at around 3400 cm^{-1} was present, corresponding to vibrations of O–H and N–H bonds from hydroxyl, carboxylic, and amine groups. The stretching of aliphatic $–CH_2$ groups was indicated by peaks at 2920–2850 cm^{-1}. A band at approximately 1720 cm^{-1} was assigned to the C=O stretching of carboxylic groups from the acrylic and crotonic acid units. The characteristic amide I band from chitosan's N-acetyl groups was observed around 1650 cm^{-1}. Other bands in the 1550–1590 cm^{-1} range were associated with N–H bending and amide II vibrations, while peaks between 1400–1450 cm^{-1} were attributed to C–N stretching and $–CH_2$ bending. Finally, the C–O–C stretching of the polysaccharide backbone was visible in the 1000–1100 cm^{-1} region. After the adsorption of dye, several noticeable changes appeared in the spectrum. The broad O–H/N–H stretching band at 3400 cm^{-1} became less intense and slightly shifted, suggesting that hydroxyl and amine groups were involved in hydrogen bonding with the dye molecules. A shift and reduction in C=O peak at 1720 cm^{-1} indicated an interaction between the composite's carboxyl groups and the dye's sulfonate groups, likely through electrostatic attraction. Furthermore, variations in the intensity of the amide bands at around 1650 cm^{-1} and 1550 cm^{-1} provided additional evidence that the amine functionalities were involved in the adsorption process [18-21].

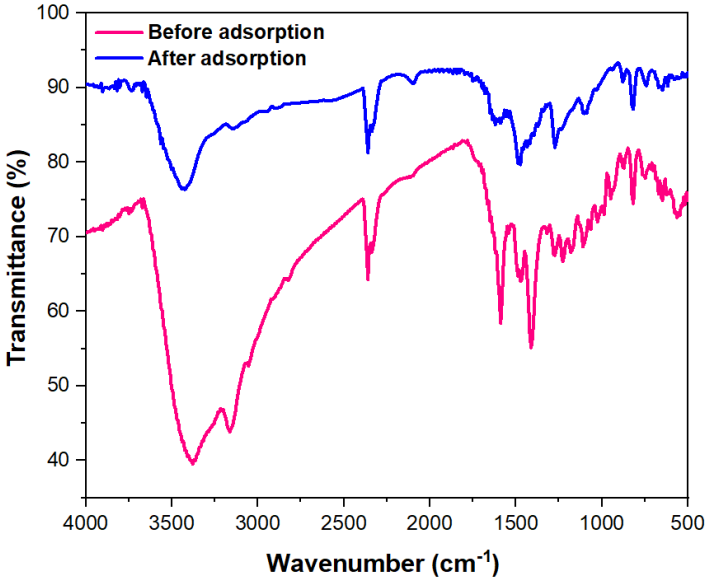

Figure 2. FTIR of prepared composite before and after dye adsorption

The XRD (**Figure 3)** of the MWCNT/Chitosan-g-P(AA–CA) composite displayed a broad peak at approximately 2θ≈20–25 °. This peak is associated with the amorphous nature of both the chitosan and the polymer graft, while also incorporating the characteristic (002) reflection from the graphitic layers of the MWCNTs. Sharp peaks were also evident around 26 ° and 43 °, confirming the presence of crystalline planes from the MWCNTs and their successful integration into the polymer matrix. A broad halo between 15 ° and 25 ° further highlighted the semi-crystalline structure of the biopolymer backbone. Compared to pristine MWCNTs, the overall intensity of the peaks was reduced, which suggests that the nanotubes were well-dispersed and that their regular stacking was partially disrupted by the grafting process [15,22,23].

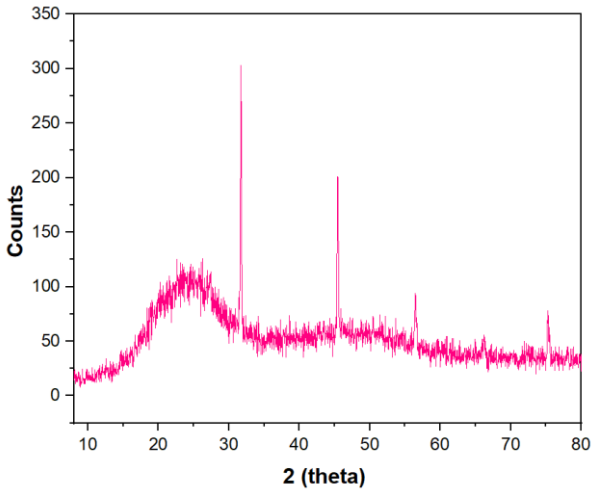

Figure 3. XRD of prepared composite

The FESEM (**Figure 4)** of the composite, taken prior to the adsorption process, revealed a surface that was rough, porous, and highly heterogeneous. The images showed that the MWCNTs were well-dispersed and effectively embedded within the polymer matrix. A significant number of cavities and channels were observed, which pointed to a large surface area and a high concentration of active binding sites available for dye molecules [24,25]. Following the adsorption of dye, a noticeable change in the surface morphology was documented. The pores and cavities that were previously visible appeared either partially or entirely filled, and the overall surface texture became smoother and more compact [12,26]. This distinct morphological

transformation provides visual evidence of the successful binding of dye molecules to the composite's surface [15,27].

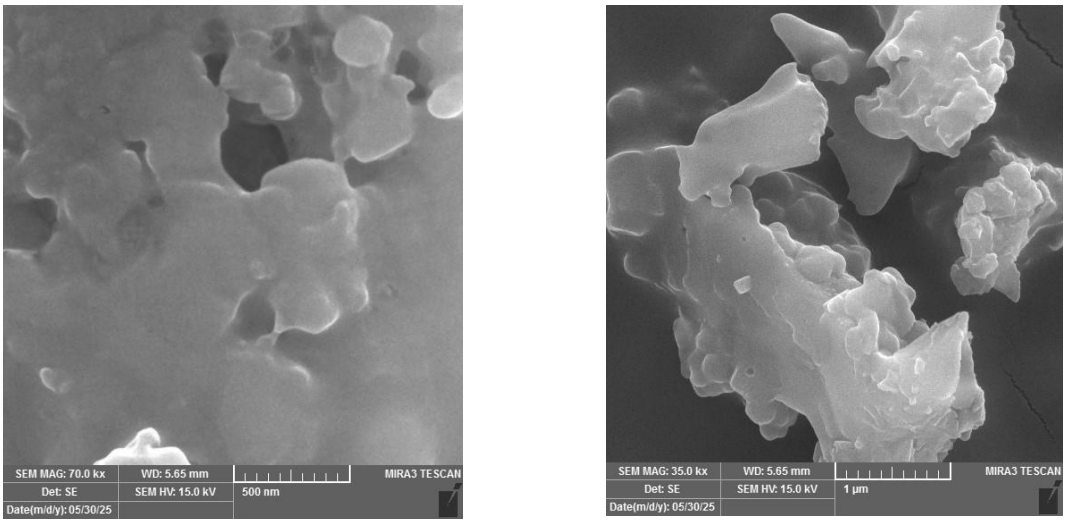

(a)

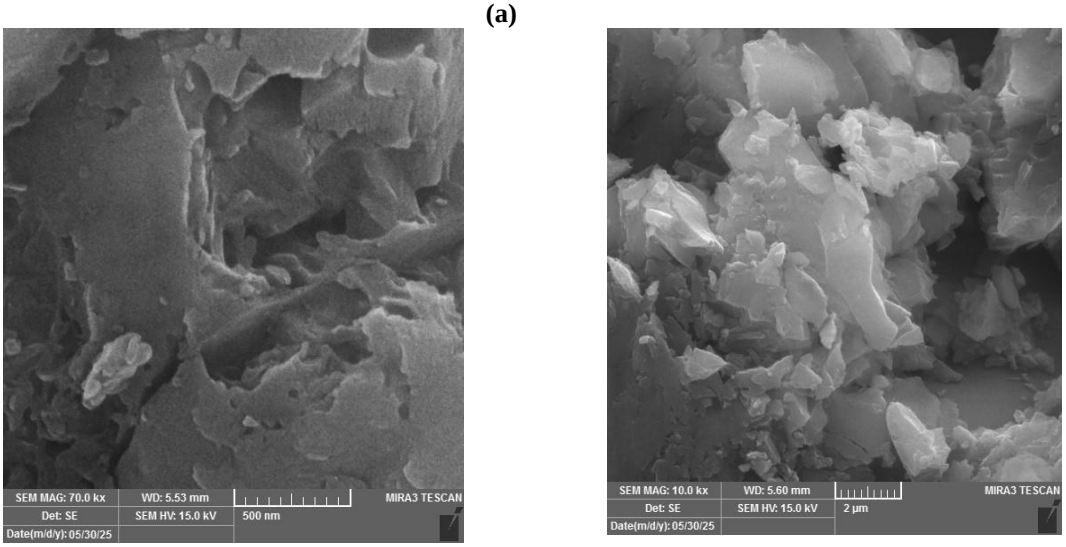

(b)

Figure 4. FESEM of prepared composite (a) before and (b) after dye adsorption

3.3. Kinetic study

The adsorption of dye onto composite was observed to be rapid during the initial minutes, which is attributed to the presence of a high number of readily available active sites. At a contact time of 1 minute, the removal efficiency was 5.39%, with a corresponding adsorption capacity of 2.70 mg/g. This efficiency then climbed sharply to 23.88% at 4 minutes, yielding a Q_e of 11.94 mg/g, and continued to rise to 30.85% at 6 minutes, resulting in a Q_e of 15.43 mg/g (**Figure 5a-d** and **Table 1**). Following this initial rapid uptake, the rate of adsorption slowed significantly, indicating that the system was approaching equilibrium as the active sites became increasingly occupied and intra-particle diffusion became the rate-limiting step. Even though the pseudo-first-order model provided a decent fit to the data (R^2 = 0.938), the pseudo-second-order model was a much better match (R^2 = 0.997). This strong agreement, along with the calculated equilibrium adsorption capacity (q_e) of 46.29 mg g^{-1} being very close to the experimental value, confirms that chemisorption is dominant rate-controlling mechanism. The kinetic data were well-described by the pseudo-first-order model, which had a good correlation coefficient (R^2) of 0.938 and a rate constant (k_1) of 0.0482 min^{-1}. This suggests that the early stages of the adsorption process were predominantly governed by physical interactions, such as

electrostatic attraction between the anionic dye and the protonated amino groups of the chitosan. Overall, the superior fit of the first-second model implies that the rate of adsorption is more take place by chemical interactions [28,29].

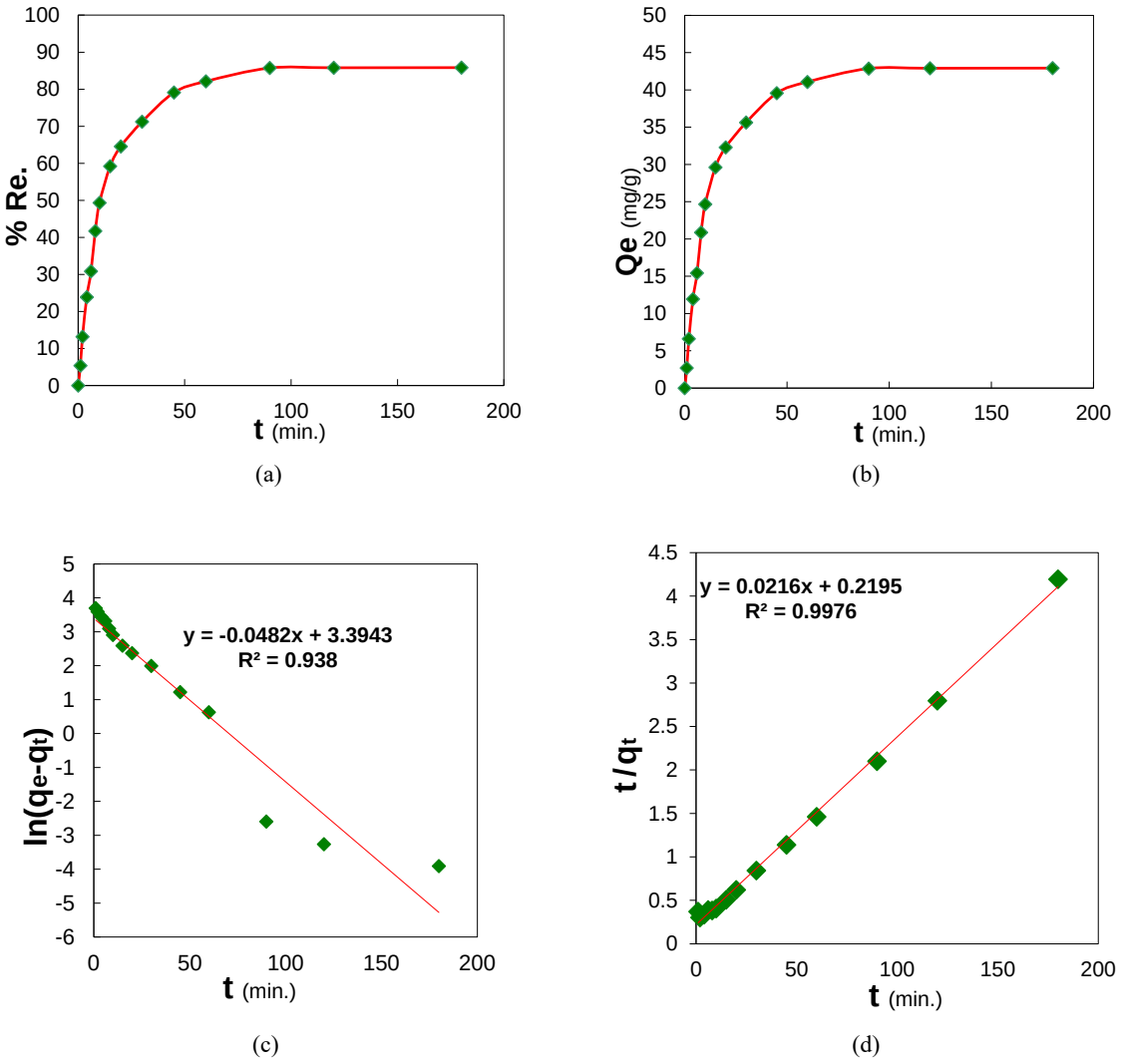

Figure 5. Effect of time on (a) removal %, (b) adsorption capacity, plot of (c) pseudo first order and (d) pseudo second order model

Table 1. Parameters obtained from pseudo first and pseudo second order model

Pseudo-first order			Pseudo-second order			
K_1 (1/min)	q_e (cal) (mg/g)	R^2	K_2	q_e (cal) (mg/g)	h	R^2
0.0482	29.79	0.938	0.0021	46.29	4.555	0.997

3.4. Thermodynamic study

Analysis of the thermodynamic parameters (**Figure 6** and **Table 2**) showed that the equilibrium constant (K_c) decreased at higher temperatures, demonstrating that the affinity of the dye for the adsorbent diminishes as the temperature rises. The negative enthalpy (ΔH) indicates that the process is exothermic, releasing heat as it occurs. The negative entropy (ΔS) shows that the system becomes more ordered and less random, as the dye molecules are immobilized on the surface. Lastly, the negative Gibbs free energy (ΔG) values confirm that the adsorption is a spontaneous process, with a greater tendency to occur at lower temperatures [30].

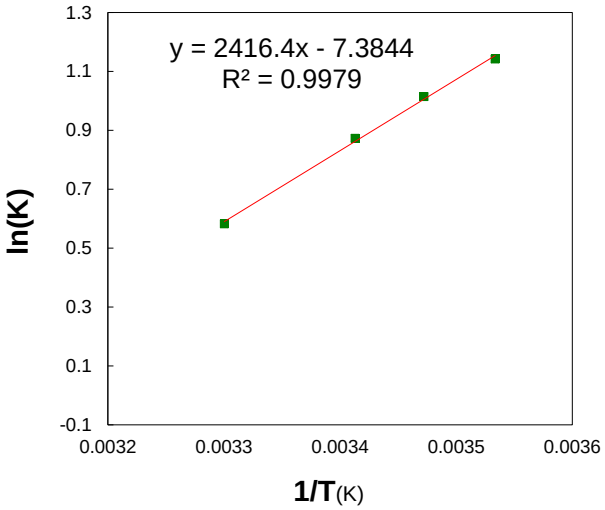

Figure 6. Van't Hoff plot

Table 2. Thermodynamic parameters

ΔH (kJ/mol)	ΔG (kJ/mol)	ΔS (kJ/K.mol)	Equilibrium Constant
-20.090	-2.127	-61.394	2.394

3.5. Effect of pH

The pH of the solution (**Figure 7**) was found to be a crucial factor influencing the adsorption capacity of the composite. At a pH of 2, the adsorption capacity was 22.98 mg/g, corresponding to a 54.04% removal efficiency. As the pH was increased to 6, the capacity rose significantly to 43.91 mg/g, achieving an 87.91% removal efficiency. This trend is explained by the protonation and deprotonation behavior of the functional groups on the adsorbent's surface. At low pH, a high concentration of H^+ ions competes with the dye anions for binding sites, thereby lowering the adsorption capacity [31,32]. In contrast, as the pH increases, this competition is reduced, and the enhanced electrostatic attraction between the negatively charged CR molecules and the positively charged adsorbent surface promotes dye uptake until the available sites become saturated [3].

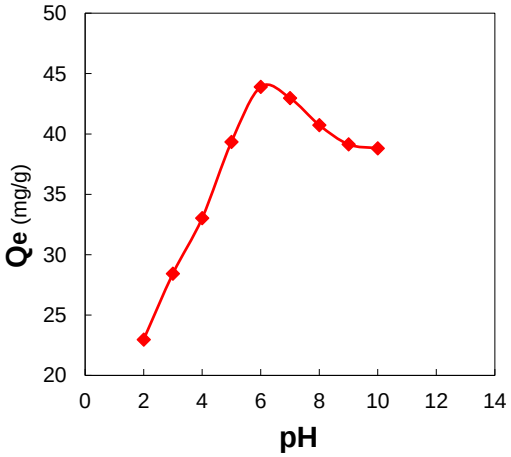

Figure 7. Effect of pH on dye adsorption

3.6. Isotherm modelling

The Q_e of composite increased as the dye dosage was raised. Concurrently, the overall percentage removal showed a slight decrease at higher concentrations. At lower initial concentrations, a large portion of the dye

molecules are successfully adsorbed due to the abundance of available binding sites, leading to a high percentage removal. However, as the concentration increases, the competition for the finite number of active sites results in a greater amount of dye being adsorbed per gram of adsorbent, thus increasing Q_e, but a lower overall percentage removal as the sites become saturated (**Figure 8a-d** and **Table 3**). The equilibrium data were best described by the Langmuir model, which suggests that the adsorption occurs as a single, uniform layer on a homogeneous surface. The q_{max} obtained from the Langmuir fit, along with the dimensionless separation factor (R_L) values being less than 1, confirms favorable nature of the adsorption. The Langmuir model also implies that all adsorption sites are energetically equivalent and that each dye molecule occupies one site without interacting with neighboring adsorbed molecules. The high adsorption capacity is likely a result of several mechanisms, including π–π stacking interactions between the aromatic rings of CR and the graphitic domains of the MWCNTs, in addition to hydrogen bonding facilitated by the chitosan and P(AA–CA) functional groups. The π–π interactions occur between graphitic surfaces of multi-walled carbon nanotubes (MWCNTs) and aromatic rings of adsorbate molecules. Simultaneously, the chitosan backbone and the grafted poly(acrylic acid–crotonic acid) polymer facilitate hydrogen bonding. Finally, at an optimal pH level, electrostatic forces also play a significant role. These three mechanisms work together to enhance the overall adsorption capacity of the material [33].

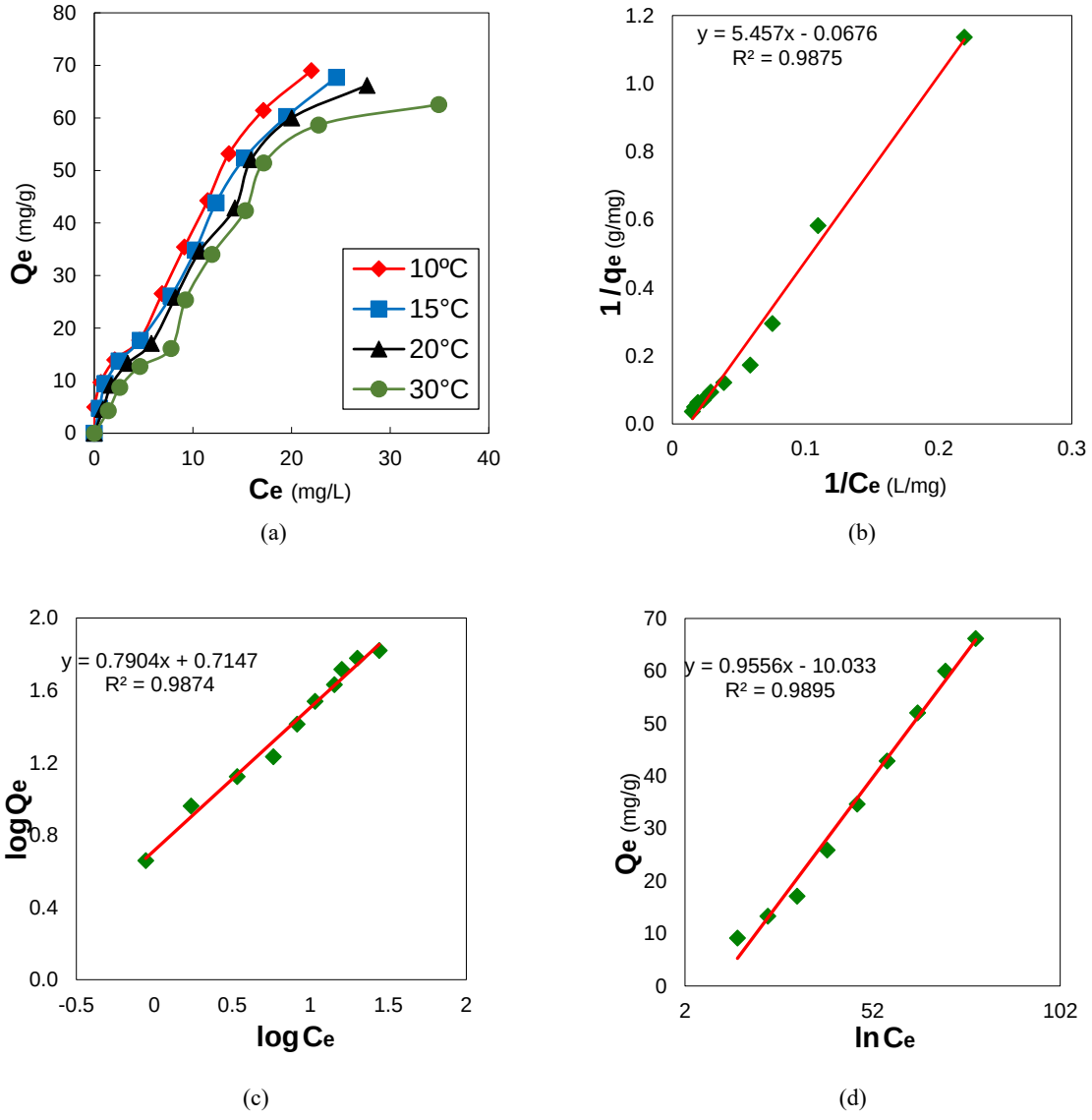

Figure 8. Effect of dye concentration on (a) adsorption capacity, plot of (b) Langmuir, (c) Freundlich and (d) Temkin model

Table 3. The Langmuir Freundlich and Temkin parameters.

Langmuir			Freundlich			Temkin		
K_L (L/mg)	q_{max} (mg/g)	R^2	K_F (mg g^{-1} (mg $L^{-1})^{-1/n}$)	1/n	R^2	K_T (L/mg)	B (J/mol)	R^2
-0.012	14.13	0.9875	5.184	0.790	0.9874	0.0001	0.9556	0.999

3.7. Effect of adsorbent dose

Increasing the adsorbent dose from 0.01 g to 0.05 g led to an increase in the percentage removal of CR from 84.06% to 87.27%. However, this increase in removal efficiency came at the cost of a significant decrease in the adsorption capacity per gram which dropped from 84.06 mg/g to 17.45 mg/g (**Figure 9a-b**). The slight improvement in removal efficiency is a direct result of the greater number of available adsorption sites provided by the larger dose. Conversely, the decrease in Q_e is attributed to the underutilization of these binding sites which reduces the total effective surface area accessible for the adsorption of dye molecules [34,35].

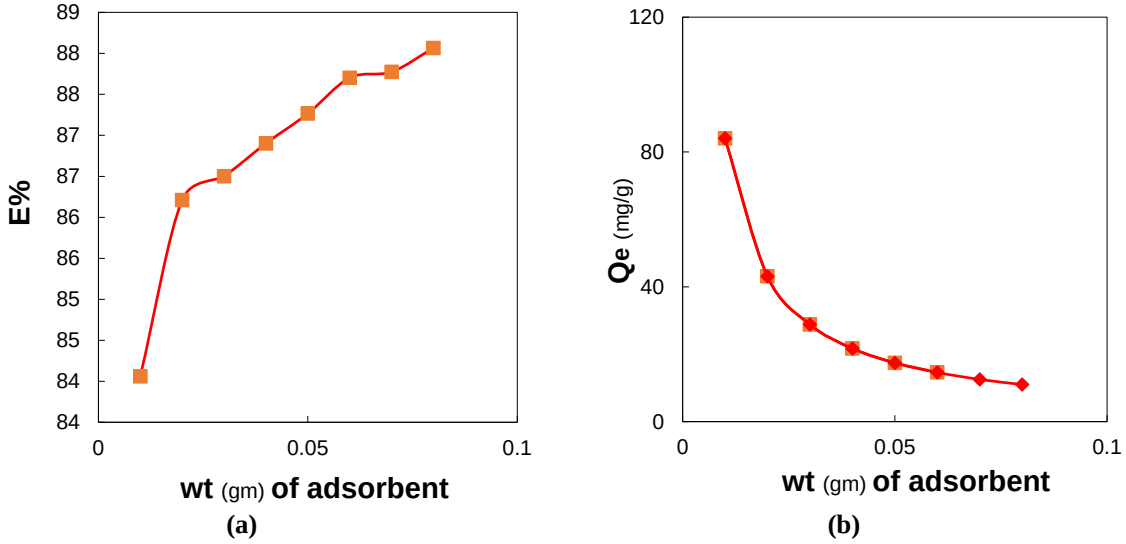

Figure 9. Effect of adsorbent dose on adsorption

4. Conclusion

In conclusion, the MWCNT/Chitosan-g-P(AA–CA) composite demonstrated outstanding performance in removing dye from solutions. Its effectiveness is attributed to its structural properties, which were confirmed through characterization to include a porous structure, high surface area, and a variety of functional groups. The adsorption process was initially very fast, reaching equilibrium in a short period, and was significantly affected by solution pH, contact time, and the amount of adsorbent used. The pseudo-second-order model was the best fit for the adsorption kinetics, which suggests that chemisorption is the primary mechanism controlling the process. Langmuir isotherm was the best fit for the equilibrium data, consistent with monolayer surface coverage. The thermodynamic findings established that adsorption was spontaneous highlighting the effective dye removal from water.

Conflict of interest

The authors declare no conflict of interest

References

1. Robinson T, McMullan G, Marchant R, Nigam P. Remediation of dyes in textile effluent: a critical review on current treatment technologies with a proposed alternative. Bioresource technology. 2001;77(3):247-55
2. Arshad R, Javed T, Thumma A. Exploring the efficiency of sodium alginate beads and Cedrus deodara sawdust for adsorptive removal of crystal violet dye. Journal of Dispersion Science and Technology. 2024;45(12):2330-43

3. Javed T, Thumma A, Uddin AN, Akhter R, Babar Taj M, Zafar S, Mahmood Baig M, Shoaib Ahmad Shah S, Wasim M, Amin Abid M. Batch adsorption study of Congo Red dye using unmodified Azadirachta indica leaves: isotherms and kinetics. Water Practice & Technology. 2024;19(2):546-66
4. ALSamman MT, Sánchez J. Chitosan-and alginate-based hydrogels for the adsorption of anionic and cationic dyes from water. Polymers. 2022;14(8):1498
5. Haider MN. Enhanced Degradation of reactive violet 1 (RV1) Dye Using Gamma and UV Irradiation Coupled with Hydrogen Peroxide. Radiation Physics and Chemistry. 2025:113191
6. Sen TK. Adsorptive removal of dye (methylene blue) organic pollutant from water by pine tree leaf biomass adsorbent. Processes. 2023;11(7):1877
7. Dur S, Husein I, Kadhim MI, Mohammed HS, Elveny M, Syah R, Hilda L. An optimally solving dentistry internal purity in heat polymerized acrylic resin with different polymerization methods. Systematic Reviews in Pharmacy. 2020;11(3):974-80.10.31838/srp.2020.3.149.
8. Kadhim MI, Jabbar AH. Synthesis of nucleotide - Amino acids via new branched chain sugar. Systematic Reviews in Pharmacy. 2020;11(6):404-8.10.31838/srp.2020.6.64.
9. Karam FF, Kadhim MI. Determination of chrysene by gas chromatography in selected soils from Al-Diwaniya province, Iraq. Asian Journal of Chemistry. 2014;26:S259-S61.10.14233/ajchem.2014.19060.
10. Gupta VK, Kumar R, Nayak A, Saleh TA, Barakat M. Adsorptive removal of dyes from aqueous solution onto carbon nanotubes: a review. Advances in colloid and interface science. 2013;193:24-34
11. Sadegh H, Zare K, Maazinejad B, Shahryari-Ghoshekandi R, Tyagi I, Agarwal S, Gupta VK. Synthesis of MWCNT-COOH-Cysteamine composite and its application for dye removal. Journal of Molecular Liquids. 2016;215:221-8
12. Alshamusi QKM, Hameed KAA, Taher AM, Batool M, Jasim LS. Efficiency of Chitosan-Grafted Poly (Carboxymethyl Cellulose-Co-Acrylamide) Nano Hydrogel for Cadmium (II) Removal: Batch Adsorption Study. Journal of Nanostructures. 2024;14(4):1122-33
13. Hussain NA, Jasim LS, editors. Kinetic Study of removal Zinc Oxide Nanoparticles from Aqueous Solutions on synthesized CH-gP (AAc-co-Am). IOP Conference Series: Earth and Environmental Science; 2021: IOP Publishing.
14. Imran MS, Javed T, Areej I, Haider MN. Sequestration of crystal violet dye from wastewater using low-cost coconut husk as a potential adsorbent. Water Science and Technology. 2022;85(8):2295-317
15. Jamel HO, Jasim MH, Mahdi MA, Ganduh SH, Batool M, Jasim LS, Haider MN. Adsorption of Rhodamine B dye from solution using 3-((1-(4-((1H-benzo[d]imidazol-2-yl)amino)phenyl)ethylidene)amino)phenol (BIAPEHB)/ P(AA-co-AM) composite. Desalination and Water Treatment. 2025;321.10.1016/j.dwt.2025.101019.
16. Bukhari A, Javed T, Haider MN. Adsorptive exclusion of crystal violet dye from wastewater by using fish scales as an adsorbent. Journal of Dispersion Science and Technology. 2023;44(11):2081-92
17. Urooj H, Javed T, Taj MB, Nouman Haider M. Adsorption of crystal violet dye from wastewater on Phyllanthus emblica fruit (PEF) powder: kinetic and thermodynamic. International Journal of Environmental Analytical Chemistry. 2024;104(19):7474-99
18. Abdulsahib WK, Sahib HH, Mahdi MA, Jasim LS. Adsorption Study of Cephalexin Monohydrate Drug in Solution on Poly (vinyl pyrrolidone-acryl amide) Hydrogel Surface. International Journal of Drug Delivery Technology. 2021;11(4):1169-72.10.25258/ijddt.11.4.9.
19. Kianipour S, Razavi FS, Hajizadeh-Oghaz M, Abdulsahib WK, Mahdi MA, Jasim LS, Salavati-Niasari M. The synthesis of the P/N-type NdCoO3/g-C3N4 nano-heterojunction as a high-performance photocatalyst for the enhanced photocatalytic degradation of pollutants under visible-light irradiation. Arabian Journal of Chemistry. 2022;15(6).10.1016/j.arabjc.2022.103840.
20. Mahdi MA, Oroumi G, Samimi F, Dawi EA, Abed MJ, Alzaidy AH, Jasim LS, Salavati-Niasari M. Tailoring the innovative Lu2CrMnO6 double perovskite nanostructure as an efficient electrode materials for electrochemical hydrogen storage application. Journal of Energy Storage. 2024;88.10.1016/j.est.2024.111660.
21. Radhy ND, Jasim LS. A novel economical friendly treatment approach: Composite hydrogels. Caspian Journal of Environmental Sciences. 2021;19(5):841-52.10.22124/cjes.2021.5233.
22. Mohammad HA, Mahde BW, Jasim LS, Batool M. Adsorption of Diclofenac Sodium (DS) Drug from Water on CMC-g-P(AAc-AAm) Nano-Hydrogel: Isotherm and Thermodynamic Study. Journal of Nanostructures. 2024;14(1):232-44.10.22052/JNS.2024.01.024.
23. Mojar Alshamusi QK, Hameed KAA, Taher AM, Batool M, Jasim LS. Efficiency of Chitosan-Grafted Poly (Carboxymethyl Cellulose-Co-Acrylamide) Nano Hydrogel for Cadmium (II) Removal: Batch Adsorption Study. Journal of Nanostructures. 2024;14(4):1122-33.10.22052/JNS.2024.04.013.
24. Abdulhusain ZH, Jasim LS, Batool M. Azur C Dye Removal using GO/P (CMC-Co-Am) Nanocomposite: Adsorption and Kinetic Studies. Journal of Nanostructures. 2024;14(4):1225-38
25. Al-Hassan HA, Salih RM, Jasim LS, Maryam B. Adsorptive Removal of Crystal Violet Dye Using Sodium Alginate-g-Poly (Acrylic Acid-Co-Itaconic Acid)/Titanium Dioxide [SA-g-p(AA-IA)/ TiO2] Hydrogel Nanocomposite. Journal of Nanostructures. 2025;15(3):1253-67.10.22052/jns.2025.03.042.

26. Alzayd AAM, Zghair AN, Essa AM, Jawad AS, Abed MJ, Batool M, Jasim LS. Isotherm and Thermodynamic Analysis of Azur C Dye Adsorption on GO/P (CMC-Co-Am) Nanocomposite. Journal of Nanostructures. 2024;14(3):845-56
27. Karim AN, Jasim LS. Synthesis and characterization of poly (CH/AA-co-AM) composite: Adsorption and thermodynamic studies of benzocaine on from aqueous solutions. International Journal of Drug Delivery Technology. 2019;9(4):558-62.10.25258/ijddt.v9i4.8.
28. Mahdi MA, Jasim LS, Mohamed MH. Synthesis and anticancer activity evaluation of novel ligand 2- [2 - (5-Chloro carboxy phenyl) Azo] 1-Methyl Imidazole (1-Mecpai) with Some Metal Complexes. Systematic Reviews in Pharmacy. 2020;11(12):1979-87.10.31838/srp.2020.12.302.
29. Alshamusi QKM, Alzayd AAM, Mahdi MA, Jasim LS, Aljeboree AM. ADSORPTION OF CRYSTAL VIOLATE (CV) DYE IN AQUEOUS SOLUTIONS BY USING P(PVP-CO-AAM)/GO COMPOSITE AS (ECO-HEALTHY ADSORBATE SURFACE): CHARACTERIZATION AND THERMODYNAMICS STUDIES. Biochemical and Cellular Archives. 2021;21:2423-31
30. Batool M, Javed T, Wasim M, Zafar S, Din MI. Exploring the usability of Cedrus deodara sawdust for decontamination of wastewater containing crystal violet dye. Desalination and Water Treatment. 2021;224:433-48
31. Qasim SM, Al-Khateeb ZT, Jabbar FA, Batool M, Jasim LS. Adsorptive and Reactivation Potential of Clay Based Superabsorbent kappa (κ)-Carrageenan-graft-Poly (Acrylic Acid-co-Acrylamide)/ Kaolin Composite for Malachite Green Dye: Linear and Non-linear modeling. Journal of Molecular Structure. 2025:143448.https://doi.org/10.1016/j.molstruc.2025.143448.
32. Saadallah K, AD C, Djedid M, Batool M, Benalia M, Saadallah S, Hamamda S. Potential of the Algerian pine tree bark for the adsorptive removal of methylene blue dye: Kinetics, isotherm and mechanism study. Journal of Dispersion Science and Technology. 2024:1-19
33. Zghair AN, Al-Khateeb ZT, Jasim LS, Batool M. Synthesis, characterization and adsorption properties of azo-functionalized polymeric hydrogels for R6G dye removal from water. Applied Chemical Engineering. 2025;8(1).10.59429/ace.v8i1.5604.
34. Alnasery H, Naseri A, Jasim LS, Sajedi-Amin S. Development and Characterization of SA-g-p(FA-AA)/GO Composite for Efficient Removal of Organic Dyes: A Step towards Water Treatment. Nanochemistry Research. 2024;9(4):351-63.10.22036/NCR.2024.04.10.
35. Alnasery H, Naseri A, Jasim LS, Sajedi-Amin S. Synthesis, characterization, and adsorption capacity of sodium alginate poly grafted (fumaric acid-co-polyacrylic acid)/graphene oxide hydrogel as adsorbent for Cr (VI) and Pb (II) removal. Journal of the Iranian Chemical Society. 2024;21(7):1915-27.10.1007/s13738-024-03037-3.